RSC Advances

PAPER

View Article Online
View Journal | View Issue

Cite this: *RSC Adv.*, 2017, 7, 2494

Crystal structure, tunable luminescence and energy transfer properties of $Na_3La(PO_4)_2:Tb^{3+},Eu^{3+}$ phosphors†

Dan Qin and Wanjun Tang*

Received 2nd November 2016
Accepted 2nd December 2016

DOI: 10.1039/c6ra26164g

www.rsc.org/advances

A series of Tb^{3+} and/or Eu^{3+} doped $Na_3La(PO_4)_2$ phosphors were successfully synthesized and their crystal structure and photoluminescence (PL) properties were investigated in detail. Double phosphates with the compositions $Na_3Tb(PO_4)_2$ and $Na_3Eu(PO_4)_2$ were obtained by the substitution of Tb or Eu for La in the $Na_3La(PO_4)_2$ host. XRD pattern analysis indicates that these obtained compounds crystallize in the orthorhombic system with the space group $Pbc2_1$. The crystal structure of the $Na_3RE(PO_4)_2$ (RE = Tb, Eu) is made up of isolated PO_4 tetrahedra and of sodium and RE atoms arranged in an ordered way. The REO_y polyhedra are isolated from one another, resulting in a high critical concentration of Tb^{3+} or Eu^{3+} activators. Under excitation of near-ultraviolet (NUV) irradiation, Tb^{3+} doped $Na_3La(PO_4)_2$ shows a blue-greenish emission with a predominant peak at 546 nm, while the emission spectra of Eu^{3+}-doped $Na_3La(PO_4)_2$ exhibits a reddish orange emission due to the $^5D_0 \rightarrow {}^7F_J$ transitions of Eu^{3+} ions. The energy transfer from Tb^{3+} to Eu^{3+} in the $Na_3La(PO_4)_2$ host is demonstrated by the luminescence spectra and fluorescence decay dynamics. Meanwhile, the emission color of $Na_3La(PO_4)_2:Tb^{3+},Eu^{3+}$ can be tuned from green to red through tuning the Tb^{3+}/Eu^{3+} ratio. These results indicate that the $Na_3La(PO_4)_2:Tb^{3+},Eu^{3+}$ phosphor exhibits broadband NUV absorption and green-reddish orange tunable emission, which might serve as a down-converting phosphor for NUV light-emitting diodes.

Introduction

Rare earth (RE) ions play an irreplaceable role in the development of lighting and display fields due to their abundant emission colors based on 4f–4f or 5d–4f transitions.[1–3] Recently, RE^{3+} ion doped phosphors based on double phosphate hosts have drawn much attention because of their high luminous efficiency, low sintering temperature, high thermal and chemical stability, and low cost.[4,5] Double phosphates of mono- and trivalent cations with the general formula $M^I{}_3N^{III}(PO_4)_2$ (M^I = Na, K; N^{III} = Y, Sc, In, Fe, rare earth elements) have high thermal and chemical stability and their host absorption edge locates at a rather short wavelength (about 140–180 nm),[6] making them excellent host materials for luminescent materials. $M^I{}_3N^{III}(PO_4)_2$ compounds crystallize in a trigonal, orthorhombic or monoclinic structure, depending on the type of M^I or N^{III} cations.[7] Among them, $Na_3RE(PO_4)_2$ (RE = La–Tb) compounds crystallize orthorhombic with the glaserite-type structure. They are built up on isolated REO_y polyhedral and PO_4 tetrahedra.[8] The presence of this particular structure suggests that the lattice can accommodate other cations with similar radii and charges without significant changes to the structural frame.[9] Furthermore, this structure can weaken the concentration quenching effect and the critical concentration of activator ions is much higher than that of conventional inorganic phosphors. Therefore, the structure and optical properties of $Na_3RE(PO_4)_2$-related phosphors have been extensively studied. A great number of glaserite-type phosphors, such as $Na_3Y(PO_4)_2:Ce^{3+}$,[10] $Na_3La(PO_4)_2:Er^{3+}$,[11] $Na_3Gd(PO_4)_2:Ce^{3+}$,[12] and $Na_3RE(PO_4)_2:Yb^{3+}$ (RE = Y, La, Gd)[13] have been reported. Meanwhile, most of the phosphors are single-colored, and combining different phosphors is applied when a multicolor emission is needed. However, this combination suffers from the disadvantages of reabsorption among phosphors and different degradation rates.[14] Therefore, great efforts have been devoted to develop single-host phosphors with a multicolor emission to meet the increasing demand of different illumination applications. In order to achieve color tunable emitting in single-phase hosts, several strategies are used, including controlling the temperature,[15] band-gap modulation,[16] crystal field adjustment,[17] the combination of multiple rare ions with various color emissions,[18] and codoping ion pairs based on the energy transfer mechanism. Codoping different rare earth ions as sensitizers and activators in a single matrix is one of the most

Hubei Key Laboratory for Catalysis and Material Science, College of Chemistry and Material Science, South-Central University for Nationalities, Wuhan 430074, P. R. China. E-mail: tangmailbox@126.com; Fax: +86-27-67842752; Tel: +86-27-67842752

† Electronic supplementary information (ESI) available: F-7000 instrumental parameters; Fig. S1 Rietveld refinement of the powder XRD pattern of $Na_3Tb_{0.95}Eu_{0.5}(PO_4)_2$; Fig. S2 Rietveld refinement of the powder XRD pattern of $Na_3Tb_{0.3}Eu_{0.7}(PO_4)_2$. See DOI: 10.1039/c6ra26164g

popular methods to control the emission color *via* energy transfer processes.[19] Additional, tunable multicolor emission can be realized in phosphors under a single excitation wavelength. The multicolor tuning of phosphors has been achieved by co-doping RE^{3+} ion into suitable host lattice, such as Eu^{3+}–Bi^{3+},[20] Tm^{3+}–Dy^{3+} (ref. 21) and Tb^{3+}–Eu^{3+}.[22–24]

It has been reported that $Na_3La(PO_4)_2$ crystallizes in the orthorhombic structure.[8] Eu^{3+} and Tb^{3+} ions are frequently used as red and green activators in luminescent materials.[19] However, the luminescence properties of Tb^{3+} and/or Eu^{3+} ions in $Na_3La(PO_4)_2$ host under near ultraviolet (NUV) light excitation have not been reported, and so far the energy transfer phenomenon from Tb^{3+} to Eu^{3+}. In this contribution, $Na_3La(PO_4)_2$ was chosen as the host material. The structure, luminescence properties and chromaticity stability of Tb^{3+} and/or Eu^{3+} activated $Na_3La(PO_4)_2$ samples are studied in detail. The energy transfer process between Tb^{3+} and Eu^{3+} ions as well as the potential luminescence mechanism has been analyzed in $Na_3La(PO_4)_2$ host upon the excitation wavelength of 378 nm irradiation.

Experimental

Powder samples of $Na_3La_{1-x}(PO_4)_2$:$x$$Eu^{3+}$ (x = 0–1.0), $Na_3La_{1-y}(PO_4)_2$:$y$$Tb^{3+}$ (y = 0–1.0), $Na_3La_{0.7-x}Tb_{0.3}(PO_4)_2$:$x$$Eu^{3+}$ (x = 0–0.7), and $Na_3La_{0.95-y}Eu_{0.05}(PO_4)_2$:$y$$Tb^{3+}$ (y = 0–0.95) were prepared as follows. Stoichiometric amounts of analytical reagents $NaNO_3$, $NH_4H_2PO_4$, and 99.99% pure La_2O_3 were mixed. An appropriate amount of $CO(NH_2)_2$ was added as fuel. 99.99% pure Eu_2O_3 and Tb_4O_7 were dissolved in HNO_3 to convert into nitrate completely. These reagents were dissolved in water and then introduced into a muffle furnace maintained at 600 °C for 5 min. The obtained processor was subsequently ground in an agate mortar and then reacted at 900 °C for 4 h in air atmosphere. Finally, the products were gradually cooled to room temperature and reground for further measurements.

The phase purity of the products was checked by powder X-ray diffraction (XRD) using a Bruker D8 X-ray diffractometer (Bruker Co. Ltd., Karlsruhe, Germany) with Cu Kα radiation (λ = 1.5406 Å), operating at 40 kV and 40 mA. Structure refinements of XRD data were performed using the computer software General Structure Analysis System (GSAS) program.[25] The luminescence emission and excitation spectra of the samples were measured on a fluorescence spectrophotometer (F-7000, Hitachi, Japan) equipped with a 150 W Xe light source. The luminescence decay data were collected on an Edinburgh FLS920 combined fluorescence lifetime and steady state spectrometer with a 450 W xenon lamp and 60 μF flash lamp. For comparison, all measurements were conducted at room temperature with the identical instrumental parameters.

Results and discussion

Phase identification and crystal structure

The XRD patterns of Tb^{3+} and/or Eu^{3+} doped $Na_3La(PO_4)_2$ samples were measured at room temperature. Fig. 1 shows the powder XRD profiles of some representative samples. No

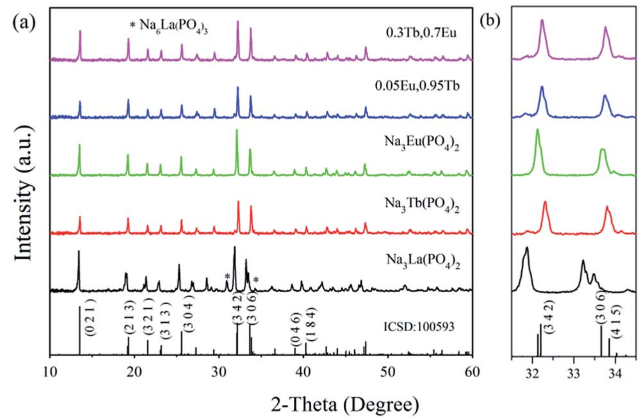

Fig. 1 Representative XRD patterns of $Na_3RE(PO_4)_2$ (RE = La, Tb, Eu) samples and ICSD no. 100593 (a); magnified XRD patterns in the region from 31.5 to 34.5 deg (b).

records of $Na_3La(PO_4)_2$, $Na_3Tb(PO_4)_2$ and $Na_3Eu(PO_4)_2$ are available in Joint Committee on Powder Diffraction Standards (JCPDS) or Inorganic Crystal Structure Database (ICSD). As shown in Table 1, the radius Nd^{3+} is quite close to that of La^{3+}, Eu^{3+} and Tb^{3+}.[26] The compound $Na_3Nd(PO_4)_2$ is isostructural with $Na_3RE(PO_4)_2$ (RE = La, Eu and Tb). Therefore, the standard data of $Na_3Nd(PO_4)_2$ (ICSD no. 100593) serve as a certified reference.[27] As presented in Fig. 1a, most of the samples are consistent with the standard file of $Na_3Nd(PO_4)_2$, indicating that the obtained samples are single phase and heavily doping Tb and/or Eu ions do not change the crystal structure. This is attributed to that Tb^{3+} or Eu^{3+} occupies La^{3+} sites for their similar radii and identical valence. However, as an exceptional case, two additional weak diffraction peaks at 30.95° and 34.27° ascribed to $Na_6La(PO_4)_3$ as a second phase can be discerned for the $Na_3La(PO_4)_2$ sample. A small shift of the XRD peaks of the $Na_3RE(PO_4)_2$ (RE = La, Eu, Tb) samples in comparison to the standard data of $Na_3Nd(PO_4)_2$ can be observed in Fig. 1b. The characteristic peak (3 4 2) shifts to the higher angle as the RE^{3+} sites are substituted by the $La^{3+} \rightarrow Nd^{3+} \rightarrow Eu^{3+} \rightarrow Tb^{3+}$ with the decrease of ionic radii. According to Bragg's diffraction equation, $2d \sin \theta = n\lambda$, in which n is an integer, λ is the X-ray wavelength, d is the spacing between the planes in the atomic lattice, and θ is the angle between the incident ray and the scattering planes. The substitution of the La^{3+} ions in the crystallographic structure by the smaller Tb^{3+} or Eu^{3+} ions reduces the cell dimensions of the crystal, leading to the increase of the 2θ value.

Table 1 The effective ionic radii of the different coordination sites of RE^{3+} in REO_y (RE = La, Nd, Eu, Tb; y = 6, 7, 8)

	Ionic radius (Å)			
y	La^{3+}	Nd^{3+}	Eu^{3+}	Tb^{3+}
6	1.032	0.983	0.947	0.923
7	1.10	—	1.01	0.98
8	1.16	1.109	1.066	1.04

Reported by Salmon *et al.*,[27] $Na_3Nd(PO_4)_2$ crystallizes in $Pbc2_1$ (no. 29) space group and orthorhombic crystal system (ICSD no. 100593). As shown in Fig. 1, solid solutions of $Na_3RE(PO_4)_2$ (RE = La, Eu and/or Tb) may exist due the same valence and similar radii of these ions.[28] Meanwhile, there are a lot of evidence about the iso-structural of orthorhombic $Na_3Nd(PO_4)_2$ with other sodium and rare-earth double orthophosphates $Na_3RE(PO_4)_2$ (RE = Y, La–Er).[10,12,29,30] Here the crystal structure data of $Na_3Nd(PO_4)_2$ is used as a starting model to refine the crystal structure. Fig. 2a and b exhibit the experimental, calculated and difference results from the Rietveld refinement of the two end components $Na_3Tb(PO_4)_2$ and $Na_3Eu(PO_4)_2$, respectively. All of the observed peaks can be indexed to the corresponding data. We can conclude that the desired single-phase phosphors with a glaserite-type structure have been synthesized and the patterns have not changed by doping Tb^{3+} and/or Eu^{3+} ions. No other phase or impurity can be detected, confirming the formation of a single phase. The low values of R_{wp}, R_p and χ^2 shown in Table 2 indicate that the refined crystal structure data are reliable. Both $Na_3Tb(PO_4)_2$ and $Na_3Eu(PO_4)_2$ crystallize in the orthorhombic crystal system with space group $Pbc2_1$ and $N = 24$. Their unit cell parameters differ from that of $Na_3Nd(PO_4)_2$ (a = 15.874 Å, b = 13.952 Å, c = 18.470 Å, V = 4090.63 Å^3), resulted from the substitution of Nd^{3+} by Tb^{3+} or Eu^{3+}. The Rietveld analysis shows that the samples are in crystalline phase and no phase mixture was observed. Rietveld plots of $Na_3Tb_{0.95}Eu_{0.5}(PO_4)_2$ and $Na_3Tb_{0.3}Eu_{0.7}(PO_4)_2$ are presented in Fig. S1 and S2 (in the ESI†), respectively. All of the observed peaks satisfy the reflection conditions, confirming the formation of a single phase with no impurities. The remarkable good fit between the experimental data and calculated line confirm the phase purity of the as-prepared samples.

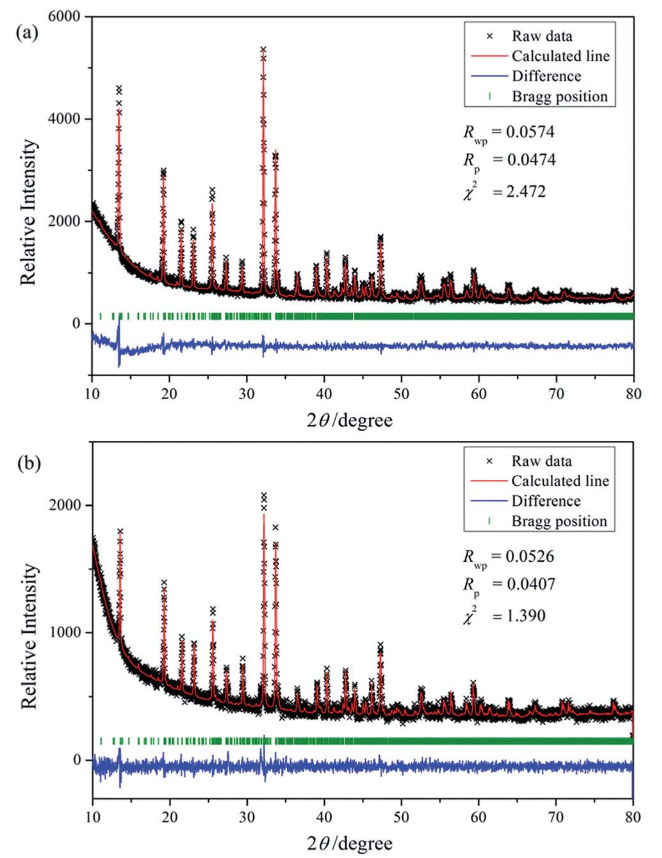

Fig. 2 Rietveld analysis patterns for X-ray powder diffraction data of $Na_3Tb(PO_4)_2$ (a) and $Na_3Eu(PO_4)_2$ (b) compounds.

Table 2 Crystallographic data and details in the data collection and refinement parameters for $Na_3RE(PO_4)_2$ (RE = Eu and Tb)

Sample	$Na_3Tb(PO_4)_2$	$Na_3Eu(PO_4)_2$
Space group	$Pbc2_1$	$Pbc2_1$
Symmetry	Orthorhombic	Orthorhombic
a/Å	15.899	15.920
b/Å	13.950	13.936
c/Å	18.405	18.425
V/Å^3	4082.1	4087.8
$\alpha = \beta = \gamma$, deg	90	90
R_{wp}, %	5.74	5.26
R_p, %	4.74	4.07
χ^2	2.472	1.390

Fig. 3a depicts the crystal structure of the $Na_3RE(PO_4)_2$ (RE = La, Eu, Tb) unit cell viewed along a-direction from the parallel projection, the coordination environment of RE^{3+} sites, and the ideal glaserite structure. The $Na_3RE(PO_4)_2$ framework is made up of isolated PO_4 tetrahedron and $[REO_y]$ (y = 6, 7, 8) polyhedron that arranged in an ordered way which results in the tunnel. The basic structure units are helical ribbons $[REO_y]$ formed by six corner sharing $[PO_4]$ tetrahedron that alternate "up" and "down.". The pinwheels are linked through $[PO_4]$ tetrahedra to form layers with alkali atoms located between the layers. Fig. 3b and c demonstrate the six kinds of RE sites in a unit cell along b-direction. The ribbons run along some

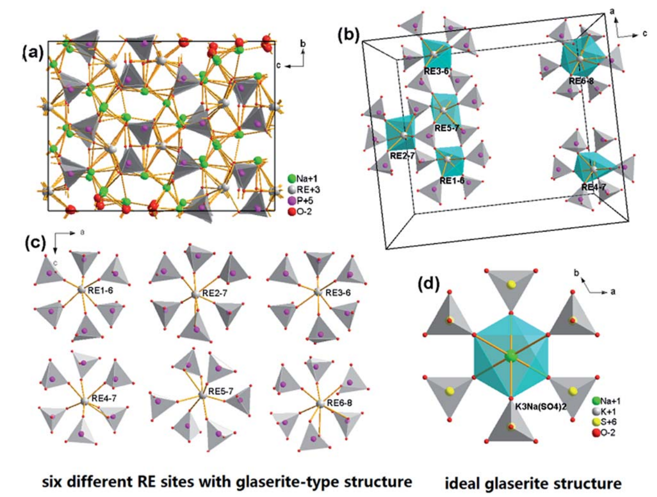

Fig. 3 Crystal structure of the $Na_3RE(PO_4)_2$ (RE = La, Eu, Tb) unit cell viewed along a-direction from the parallel projection (a); the coordination environment of different Nd^{3+} sites in a unit cell (b); the expansion particular six kinds of Nd^{3+} (c); the ideal glaserite structure of the $K_3Na(SO_4)_2$ (d).

directions of unit-cell with a period of four or eight tetrahedral. The coordination of the RE atoms is 6-folded for RE1 and RE3, 7-folded for RE2, RE4, RE5 and 8-folded for RE6. The variety in coordination numbers is due to a rotation of the certain [PO_4] tetrahedron around one of their edges. The REO_y polyhedral are isolated because they do not share any O atom. In addition, the shortest RE–RE distances in $Na_3Tb(PO_4)_2$ and $Na_3Eu(PO_4)_2$ are about 4.641 and 4.646 Å (RE2–RE5), respectively, which is a long distance that energy migration of the doped rare earth ions is difficult, similar observation has also been witnessed in some systems such as $Na_3Gd_{1-x}Eu_x(PO_4)_2$ (ref. 31) and $Na_3Gd(PO_4)_2$:Ce^{3+}.[12]

Luminescence properties of Tb^{3+} and/or Eu^{3+} doped $Na_3La(PO_4)_2$ phosphors

Fig. 4 illustrates the UV-vis excitation (PLE, $\lambda_{em} = 546$ nm) and emission (PL, $\lambda_{em} = 378$ nm) spectra of $Na_3La_{1-x}(PO_4)_2$:xTb^{3+} with $x = 0.01$–1.0. The PLE spectrum of $Na_3Tb(PO_4)_2$ involves several sharp lines in the 280–420 nm range. The sharp f–f excitation lines at about 302, 317, 340, 351, 358, 368, 378 and 486 nm are assigned to $^7F_6$–$^5H_6$, $^7F_6$–$^5H_7$, $^7F_6$–$^5G_2$, $^7F_6$–$^5D_2$, $^7F_6$–$^5L_{10}$, $^7F_6$–$^5G_6$ and $^7F_6$–$^5D_4$, respectively.[31] Under 378 nm NUV excitation, the PL spectrum of $Na_3La_{0.99}(PO_4)_2$:$0.01Tb^{3+}$ presents a group of $^5D_{3,4} \rightarrow {}^7F_J$ transitions: $^5D_3 \rightarrow {}^7F_5$ (415 nm), $^5D_3 \rightarrow {}^7F_4$ (437 nm), $^5D_4 \rightarrow {}^7F_6$ (490 nm), $^5D_4 \rightarrow {}^7F_5$ (546 nm), $^5D_4 \rightarrow {}^7F_4$ (586 nm) and $^5D_4 \rightarrow {}^7F_3$ (623 nm). With the increase of Tb^{3+} concentration (x), the blue emissions from the $^5D_3 \rightarrow {}^7F_{5,4}$ transitions are quenched gradually, while the green emissions from the $^5D_4 \rightarrow {}^7F_{6,5,4,3}$ transitions increase continuously. For the Tb^{3+} ion, the energy gap between the $^5D_3$ and $^5D_4$ levels is about 5915 cm^{-1}, which is quite close to that between $^7F_6$ and $^7F_0$ levels (6000 cm^{-1}).[32] Hence, if the Tb^{3+} concentration (y) is high enough, the emission from the $^5D_3$ level of Tb^{3+} is much weaker than that from the $^5D_4$ level due to the cross relaxation *via* the resonant energy transfer process: Tb^{3+} ($^5D_3$) + Tb^{3+} ($^7F_6$) → Tb^{3+} ($^5D_4$) + Tb^{3+} ($^7F_0$) and the green emission of the $^5D_4 \rightarrow {}^7F_5$ (546 nm) becomes predominant.[33] The PL intensity of Tb^{3+} $^5D_4 \rightarrow {}^7F_5$ transition increases gradually with its concentration (x) increasing, and reaches a maximum at $x = 1$. This result indicates that no concentration quenching exists in the $Na_3La(PO_4)_2$ host among the Tb^{3+} ions. The $Na_3Tb(PO_4)_2$ sample shows strong green emission under 378 nm NUV irradiation excitation, which makes it be a potential green phosphor for NUV LED application.

The PLE spectrum of $Na_3Eu(PO_4)_2$ and PL spectra of $Na_3La_{1-y}(PO_4)_2$:yEu^{3+} ($y = 0.01$–1.0) are shown in Fig. 5. The PLE spectrum consists of a weak broad band assigned to the charge-transfer transition (CTB) between Eu^{3+} and O^{2-}, some narrow lines in the range of 230–320 nm (the strongest peak located at about 306 nm is due to Rayleigh scattering), and several sharp lines from 360–480 nm. These sharp lines correspond to the characteristic f → f transitions of Eu^{3+} ions within its $4f^6$ configuration. They are ascribed to $^7F_0 \rightarrow {}^5D_4$ (360 nm), $^7F_0 \rightarrow {}^5G_J, {}^5L_7$ (381 nm), $^7F_0 \rightarrow {}^5L_6$ (394 nm), $^7F_0 \rightarrow {}^5D_3$ (414 nm), and $^7F_0 \rightarrow {}^5D_2$ (464 nm) transitions of Eu^{3+} ion, respectively. Excitation into the $^7F_0 \rightarrow {}^5L_6$ transition of Eu^{3+} at 394 nm yields some characteristic emission lines from the $^5D_{0,1}$ excited states to the ^7F_J ground states, *i.e.*, $^5D_1 \rightarrow {}^7F_1$ (536 nm), $^5D_1 \rightarrow {}^7F_2$ (556 nm), $^5D_0 \rightarrow {}^7F_1$ (594 nm), $^5D_0 \rightarrow {}^7F_2$ (620 nm), $^5D_0 \rightarrow {}^7F_3$ (655 nm), and $^5D_0 \rightarrow {}^7F_4$ (703 nm), respectively.[34] However, the $^5D_0 \rightarrow {}^7F_0$ transition (about 580 nm) is very weak and can hardly be detected.

The two dominant bands at 594 ($^5D_0 \rightarrow {}^7F_1$ transition) and 620 nm ($^5D_0 \rightarrow {}^7F_2$ transition) confer on the sample an orange-red luminescence upon excitation with 394 nm light. It is known that the magnetic-dipole transition $^5D_0 \rightarrow {}^7F_1$ is insensitive to the symmetry of the Eu^{3+} site, while the forced electric dipole transition $^5D_0 \rightarrow {}^7F_2$ is hypersensitive to the local environment.[35,36] Therefore, the intensity ratio (R) of ($^5D_0 \rightarrow {}^7F_2$)/($^5D_0 \rightarrow {}^7F_1$) gives a measure of the Eu^{3+} site symmetry in the lattice. A higher value of R ($R > 1$) suggests that Eu^{3+} locates at the site without inversion symmetry. Otherwise, Eu^{3+} ion locates at the site with inversion symmetry, leading to a lower value of R ($1 > R > 0$).[37] As shown in Fig. 3d, Na^+ has an inversion symmetric environment in the ideal glaserite structure of $K_3Na(SO_4)_2$. However, upon substitution of Na^+ sites by RE^{3+},

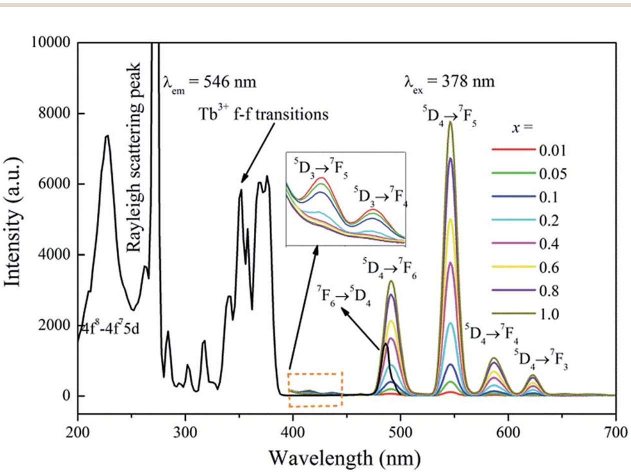

Fig. 4 The PLE spectrum of $Na_3Tb(PO_4)_2$ and the PL spectra of $Na_3La_{1-x}(PO_4)_2$:xTb^{3+} ($x = 0.01$–1.0) samples.

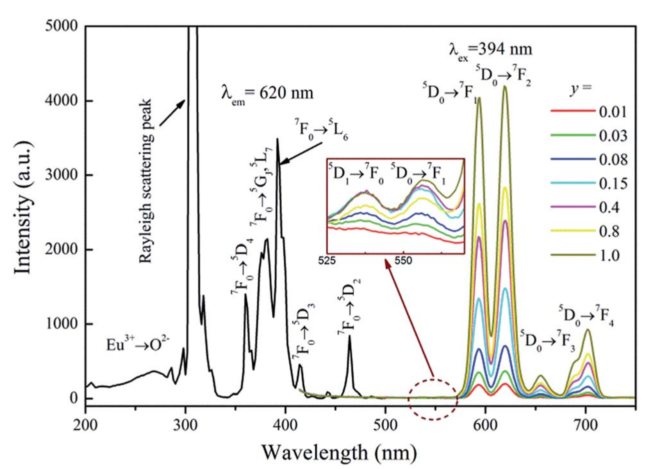

Fig. 5 The PLE spectrum of $Na_3Eu(PO_4)_2$ and the PL spectra of $Na_3La_{1-y}(PO_4)_2$:yEu^{3+} ($y = 0$–1) samples.

there will be some distortion in NaO_6 octahedron. The $Na_3RE(PO_4)_2$ structure seems to be a distorted glaserite structure. In this structure six different types of REO_y polyhedral can be expected. Hence, the Eu^{3+} ion may occupy six sites in the $Na_3RE(PO_4)_2$ lattice, as shown in Fig. 3b and c. Here, the intensity of $^5D_0 \rightarrow {}^7F_1$ is comparable with that of $^5D_0 \rightarrow {}^7F_2$. The value of R calculated is about 1.02, indicating that the Eu^{3+} ions occupies a symmetric and a non-symmetric site almost equally. This agrees with the results of Eu^{3+} doped $K_3Y(PO_4)_2$ (ref. 34) and $Na_3Y(PO_4)_2$ (ref. 38) but challenges the results of Eu^{3+} doped $Rb_3Y_2(PO_4)_3$ and $Rb_3La(PO_4)_2$.[39]

The PL intensity ($^5D_0 \rightarrow {}^7F_2$) of $Na_3La_{1-y}(PO_4)_2$:$y$$Eu^{3+}$ increases with increasing Eu^{3+} concentration (y) until a maximum intensity about $y = 1.0$ is reached. These observations confirm that the concentration quenching of Eu^{3+} does not occur in $Na_3La(PO_4)_2$ host, so highly doping concentration samples are performed here.

It is worthy to be noted that both $Na_3La_{1-x}(PO_4)_2$:$x$$Tb^{3+}$ and $Na_3La_{1-y}(PO_4)_2$:$y$$Eu^{3+}$ phosphors have a much high quenching concentration, actually the complete quenching would not occur even at x or $y = 1.0$, at which the La^{3+} sites are replaced by Tb^{3+} or Eu^{3+} completely. Taking into account the inherent structural feature of $Na_3RE(PO_4)_2$ host, in which the Tb^{3+} or Eu^{3+} ions occupy the RE^{3+} sites of polyhedral which isolate from each other by a large spatial distance and join by RE–O–P–O–RE. The large spatial distance between RE^{3+} ions and the shielding of PO_4 tetrahedrons hinders the long range energy transfer between Tb^{3+} or Eu^{3+} ions and consequently prevents the occurrence of concentration quenching. Therefore, the high concentration quenching was observed in $Na_3La_{1-x}(PO_4)_2$:$x$$Tb^{3+}$ and $Na_3La_{1-y}(PO_4)_2$:$y$$Eu^{3+}$ phosphors. The similar phenomenon was also reported by Chen *et al.* in $K_3R(PO_4)_2$:Tb^{3+} (R = Y and Gd) phosphors,[40] Ju *et al.* in $Na_3Gd_{1-x}Eu_x(PO_4)_2$ phosphors,[30] and Jiang *et al.* in $K_3Gd(PO_4)_2$:Tb^{3+},Eu^{3+} phosphor.[41]

In order to obtain multicolor tunable luminescence of the $Na_3La(PO_4)_2$ phosphor, Tb^{3+} and Eu^{3+} ions with different relative concentration into the $Na_3La(PO_4)_2$ host lattice were codoped in our work. The PLE and PL spectra of the $Na_3La_{0.65}(PO_4)_2$:0.3Tb^{3+},0.05Eu^{3+} sample are shown in Fig. 6. For comparison, the PLE and PL spectra of $Na_3Tb(PO_4)_2$ and $Na_3Eu(PO_4)_2$ are also presented. The PLE spectrum (Fig. 6c) of the $Na_3La_{0.65}(PO_4)_2$:0.3Tb^{3+},0.05Eu^{3+} by monitoring the emission of Tb^{3+} at 546 nm is almost identical to that of $Na_3Tb(PO_4)_2$ (Fig. 6a) within the experimental error. The PLE band/line of Eu^{3+} is undetectable, implying that Eu^{3+} cannot transfer energy to Tb^{3+}. The PLE spectrum recorded at the 620 nm of Eu^{3+} emission is dominated by Tb^{3+} bands/lines, which are similar to that of monitoring the Tb^{3+}-emission, but shows large difference with that of Eu^{3+} (Fig. 6b). Only several f–f transition lines of Eu^{3+} are evidently observed (marked by stars in Fig. 6c). The presence of Tb^{3+}-related PLE bands/lines in the PLE spectrum of Eu^{3+} emission clearly indicates the occurrence of energy transfer from Tb^{3+} to Eu^{3+}. Upon 394 nm excitation ($^7F_0 \rightarrow {}^5L_6$ of Eu^{3+}), only emission from Eu^{3+} is observed, and the positions of all emission peaks are identical to those in Fig. 6b of $Na_3Eu(PO_4)_2$. Excited at 378 nm UV irradiation ($^7F_6 \rightarrow {}^5G_6$ of Tb^{3+}), the characteristic sharp emissions from both Eu^{3+} and Tb^{3+} can be detected, confirming that Tb^{3+} can partially transfer excitation energy to Eu^{3+} *via* its absorption of 4f state. Therefore, the relative intensities of these two emissions can be varied by adjusting the concentrations of the two activators through the principle of energy transfer.

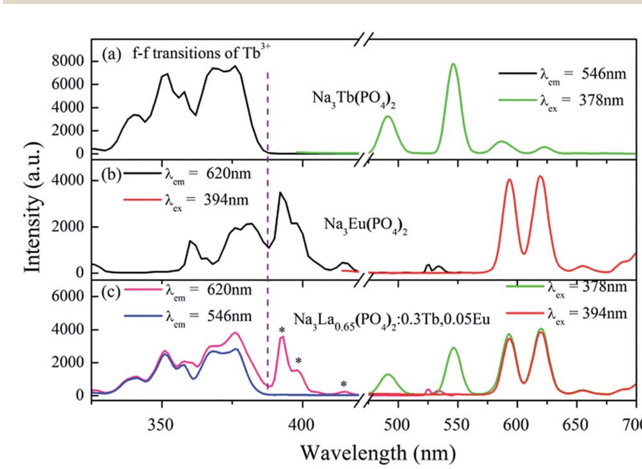

Fig. 6 PLE and PL spectra of $Na_3Tb(PO_4)_2$ (a), $Na_3Eu(PO_4)_2$ (b), and $Na_3La_{0.65}(PO_4)_2$:0.3Tb^{3+},0.05Eu^{3+} (c).

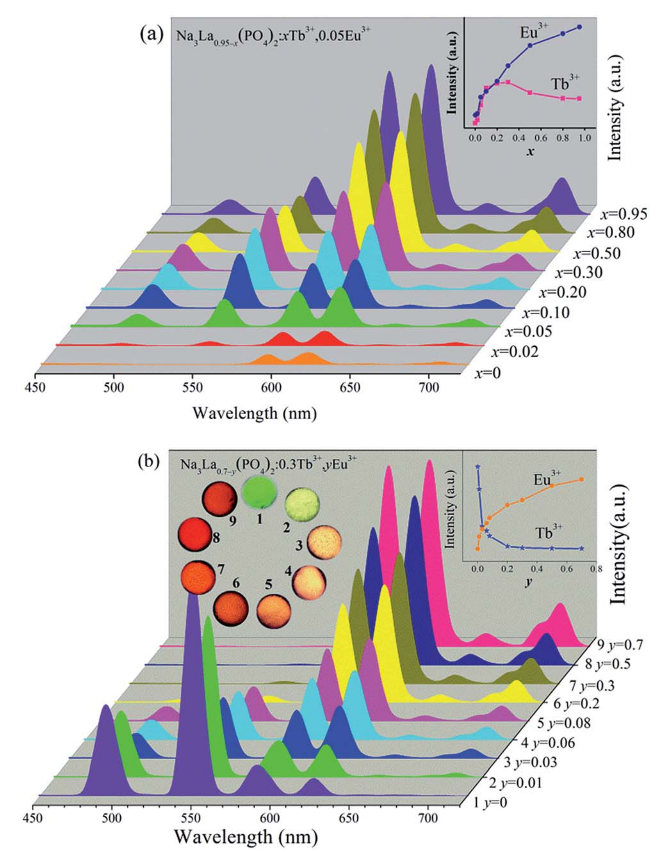

Fig. 7 PL spectra (λ_{ex} = 378 nm) of $Na_3La_{0.95-x}(PO_4)_2$:$x$$Tb^{3+}$,0.05$Eu^{3+}$ (x = 0–0.95, *a*) and $Na_3La_{0.7-y}(PO_4)_2$:0.3Tb^{3+},$y$$Eu^{3+}$ (y = 0–0.7, *b*) phosphors together with their digital photographs under a 365 nm UV lamp.

Fig. 7 illustrates the variations of PL spectra and corresponding intensities of $Na_3La_{0.95-x}(PO_4)_2$:$x$$Tb^{3+}$,0.05$Eu^{3+}$ and $Na_3La_{0.7-y}(PO_4)_2$:0.3Tb^{3+},$y$$Eu^{3+}$ phosphors. The emission profile of all the Tb^{3+}/Eu^{3+} codoped samples contain the characteristic sharp emission peaks of both Tb^{3+} and Eu^{3+} under excitation at 378 nm. The increasing concentrations of the Eu^{3+} or Tb^{3+} ions bring no obvious alteration in the intensity ratio of ($^5D_0 \rightarrow {}^7F_2$)/($^5D_0 \rightarrow {}^7F_1$), indicating that the degree of the local symmetry around Eu^{3+} ions keeps constant. As shown in Fig. 7a, the PL intensities of Eu^{3+} at 620 nm increase systematically with increasing the Tb^{3+} concentration (x), because the increase of Tb^{3+} concentration results in more sensitizers transferring the energy to Eu^{3+} ions. Meanwhile, the Tb^{3+} green emission intensity reaches its maximum at $x = 0.3$, and then decreases due to the concentration quenching effect with further increasing the Tb^{3+} concentration (x). The inset of Fig. 7a depicts the dependences of the PL intensities (($^5D_4 \rightarrow {}^7F_5$ transition of Tb^{3+}; $^5D_0 \rightarrow {}^7F_2$ transition of Eu^{3+}; $\lambda_{ex} = 378$ nm)) on the Tb^{3+} concentration (y). The Eu^{3+} PL intensity is enhanced about 11 times by codoping with Tb^{3+}. In Fig. 7b, the PL intensity of Tb^{3+} decreases monotonously with the increase of Eu^{3+} concentration from $y = 0$ to 0.7, while the Eu^{3+} PL intensity increases to a maximum at $y = 0.7$. This observation indicates that the energy transfer from Tb^{3+} to Eu^{3+} ions can occur in current excitation condition in Tb^{3+}/Eu^{3+} codoped $Na_3La(PO_4)_2$ phosphor. Therefore, the relative intensities of these two emissions can be varied by adjusting the concentrations of the two activators through the principle of energy transfer to realize the tunable emission color. The digital emission color photos were depicted in the inset of Fig. 7b, clearly indicating that the emission color can be tuned from green to reddish orange with increasing the Eu^{3+} concentration (y).

Decay curves and energy transfer mechanism

It has been witnessed that an efficient energy transfer from Tb^{3+} to Eu^{3+} occurs in $Na_3La(PO_4)_2$ host. In order to further investigate the energy transfer between Tb^{3+} and Eu^{3+} in $Na_3La(PO_4)_2$, luminescent decay curves of Tb^{3+} emission and Eu^{3+} emission in $Na_3La_{0.7-y}(PO_4)_2$:0.3Tb^{3+},$y$$Eu^{3+}$ ($y = 0$–0.7) samples have been measured. The decay curves monitored at 546 nm (Tb^{3+} $^5D_4 \rightarrow {}^7F_5$ transition) and 620 nm (Eu^{3+} $^5D_0 \rightarrow {}^7F_5$ transition) with excitation of 378 nm irradiation are presented in Fig. 8a and b, respectively.

It is found that the decay curves of Tb^{3+} emission cannot be fitted in terms of a single-exponential function, but can be well fitted by a double-exponential function:

$$I = A_1 \exp(-t/\tau_1) + A_2 \exp(-t/\tau_2) \quad (1)$$

where I is the luminous intensity at time t; A_1 and A_2 are the fitting parameters; and τ_1 and τ_2 are rapid and slow lifetimes for exponential components, respectively. The decay process of these samples is characterized by an effective lifetime τ, which can be calculated using eqn (2) as follows

$$\tau = (A_1\tau_1^2 + A_2\tau_2^2)/(A_1\tau_1 + A_2\tau_2) \quad (2)$$

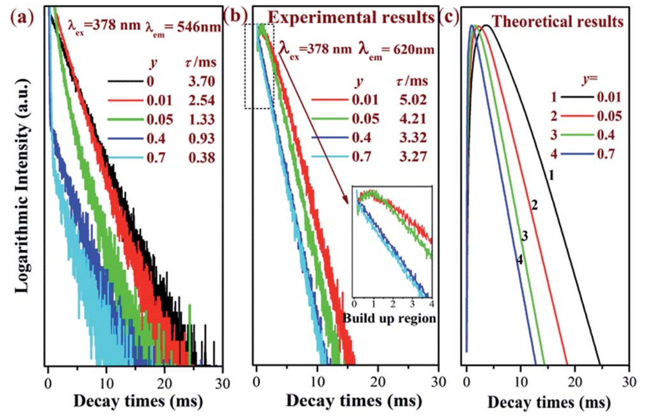

Fig. 8 Luminescence decay curves of Tb^{3+} 546 nm emission ($^5D_4 \rightarrow {}^7F_5$) (a), Eu^{3+} 620 nm emission ($^5D_0 \rightarrow {}^7F_5$) (b) and the corresponding simulation curves (c).

The values of τ_{Tb} are calculated to be 3.70, 2.54, 1.33, 0.93 and 0.38 ms for $Na_3La_{0.7-y}(PO_4)_2$:0.3Tb^{3+},$y$$Eu^{3+}$ phosphors with $y = 0$, 0.01, 0.05, 0.4 and 0.7. As shown in Fig. 9, the effective lifetime of Tb^{3+} ions decreases with the increase of Eu^{3+} due to the $ET_{Tb\rightarrow Eu}$ process.

For the $ET_{Tb\rightarrow Eu}$ process, the transfer probability ($P_{Tb\rightarrow Eu}$) can be expressed by eqn (3)[42]

$$P_{Tb\rightarrow Eu} = 1/\tau - 1/\tau_0 \quad (3)$$

where $P_{Tb\rightarrow Eu}$ is the energy transfer probability and τ and τ_0 are the lifetimes for Tb^{3+} with and without the Eu^{3+} ions, respectively. In addition, the energy transfer efficiency ($\eta_{Tb\rightarrow Eu}$) can be evaluated using eqn (4),

$$\eta_{Tb\rightarrow Eu} = 1 - \tau/\tau_0 \quad (4)$$

The values of $P_{Tb\rightarrow Eu}$ and $\eta_{Tb\rightarrow Eu}$ are calculated and are also shown in Fig. 9. Both the values of $P_{Tb\rightarrow Eu}$ and $\eta_{Tb\rightarrow Eu}$ increase obviously with increasing the Eu^{3+} concentration (y), indicating that the energy-transfer process become more efficient with high Eu^{3+} ion concentration.

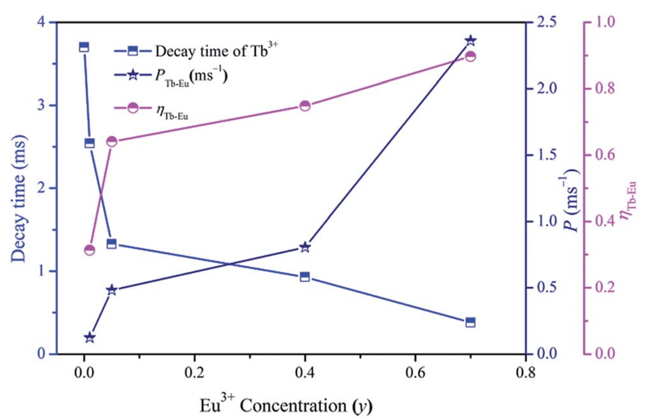

Fig. 9 Dependence of Tb^{3+} decay time, $P_{Tb\rightarrow Eu}$ and $\eta_{Tb\rightarrow Eu}$ on Eu^{3+} concentration (y) in $Na_3La_{0.7-y}(PO_4)_2$:0.3Tb^{3+},$y$$Eu^{3+}$.

Fig. 8b illustrates the decay curves of Eu^{3+} emission. All the decay curves of Eu^{3+} emission could be well fitted into singly exponential equation

$$I_t = I_0 \exp(-t/\tau) \quad (5)$$

where I_0 and I_t are for the intensities of Eu^{3+} emission at time t_0 and t, respectively; τ denotes the lifetimes for Eu^{3+}. The calculated values of τ_{Eu} are 5.02, 4.21, 3.32 and 3.27 ms for $y = 0.01$, 0.05, 0.4 and 0.7 in $Na_3La_{0.7-y}(PO_4)_2$:$0.3Tb^{3+}$,yEu^{3+} phosphors.

It is obvious that the Eu^{3+} decay curves recorded at the $^5D_0 \rightarrow {}^7F_5$ transition (620 nm) exhibit a rising step. The fluorescence intensity increases with increasing time, then reaching a maximum, and finally decreases until the decay process completes. Therefore, there are two different processes for the emission of Eu^{3+}: decay process and build-up process. In the initial build-up process, the energy absorbed by the $^7F_6 \rightarrow {}^5G_6$ transition of Tb^{3+} ions is transferred to Eu^{3+} ions. This process is significantly influenced by the Eu^{3+} concentration. As shown in Fig. 8b, with increasing the Eu^{3+} concentration (y), the initial build-up process becomes faster and faster, suggesting that the $ET_{Tb\rightarrow Eu}$ process becomes more efficient with higher Eu^{3+} concentration.[43] When the $Na_3La_{0.7-y}(PO_4)_2$:$0.3Tb^{3+}$,yEu^{3+} samples are excited by 378 nm irradiation, the rate equations for the population densities in the $^5D_4$ level of Tb^{3+} and the $^5D_0$ of Eu^{3+} ion can be expressed as follows,[44]

$$dN_{Tb}/dt = -N_{Tb}/\tau_{Tb} - K_{Tb-Eu}N_{Tb} \quad (6)$$

$$dN_{Eu}/dt = -N_{Eu}/\tau_{Eu} + K_{Tb-Eu}N_{Tb} \quad (7)$$

where the N_{Tb} and N_{Eu} are the population intensities of the $^5D_4$ level of Tb^{3+} and the $^5D_0$ of Eu^{3+}, respectively. K_{Tb-Eu} is the non-radiative energy transfer rate from the $^5D_4$ state of Tb^{3+} to $^5D_0$ of Eu^{3+}. Then the fluorescence intensity $I(t)$ of Eu^{3+} ions at 620 nm excited at 378 nm irradiation can be given as following equation:

$$I(t) = N_{Eu}(t) = N_{Eu}/\tau_{Eu} = \frac{K_{Tb-Eu}N_{Tb}}{1/\tau_{Eu} - 1/\tau_{Tb}}\left[\exp\left(-\frac{t}{\tau_{Tb}}\right) - \exp\left(-\frac{t}{\tau_{Eu}}\right)\right] \quad (8)$$

Using the measured values of τ_{Tb} and τ_{Eu}, the simulation curves for $Na_3La_{0.7-y}(PO_4)_2$:$0.3Tb^{3+}$,yEu^{3+} samples are obtained as presented in Fig. 8c, which show two process for Eu^{3+} emission, being similar to the measured curves. That is to say, the theoretical results are consistent with the experimental observations.

In general, the energy transfer between the sensitizer and activator may take place *via* exchange interaction and multipolar interaction. The energy transfer mechanism can be determined using the following relationship:[45]

$$\ln(I_0/I) \propto C \text{ and } I_{S0}/I_S \propto C^{\alpha/3} \quad (9)$$

in which I_{S0} and I_S are the luminescence intensities of Tb^{3+} in the absence and presence of Eu^{3+}, respectively; C is the total concentration of Tb^{3+} and Eu^{3+}; $\ln(I_{S0}/I_S) \propto C$ is corresponding to the exchange interaction; $\alpha = 6$, 8, and 10 are dipole–dipole, dipole–quadrupole, and quadrupole–quadrupole interactions. The relationships are illustrated in Fig. 10a–d, respectively for $Na_3La_{0.7-y}(PO_4)_2$:$0.3Tb^{3+}$,yEu^{3+} phosphors. The linear behavior was observed only when $\alpha = 6$, indicating that energy transfer from Tb^{3+} to Eu^{3+} in $Na_3La(PO_4)_2$ host occurs *via* a dipole–dipole interaction.

The scheme of energy transfer from Tb^{3+} to Eu^{3+} in $Na_3La(PO_4)_2$ host is demonstrated in Fig. 11. Tb^{3+} ions absorb the energy from 378 nm irradiation and are excited from the ground state of ($^7F_6$) to the excited states of ^5D_J ($J = 2, 3, 4$). Some of the excited Tb^{3+} radiative transmit from $^5D_3$ to the ground state $^7F_6$ directly with relatively weaker blue light emission of 415 and 437 nm, and other excited Tb^{3+} relax to the lowest excited state $^5D_4$ through non-radiative transition, then radiative decay to the ground state ($^7F_6$) with a strong green emission. When Eu^{3+} ions are codoped, part of the energy from $^5D_4$ to ^7F_J transition of Tb^{3+} will be transferred to Eu^{3+} through cross-relaxation due the obvious overlap between the $^5D_4 \rightarrow {}^7F_J$ emission of Tb^{3+} and $^7F_{0,1} \rightarrow {}^5D_{0,1,2}$ absorption of Eu^{3+}, then relax to the ground state $^5D_0$ of Eu^{3+} and finally radiative decay to the ground state ($^7F_0$) with an reddish orange emission.[44]

CIE chromaticity coordinates of $Na_3La(PO_4)_2$:Tb^{3+},Eu^{3+}

The CIE chromaticity coordinates (X, Y) for $Na_3La_{0.7-y}(PO_4)_2$:$0.3Tb^{3+}$,yEu^{3+} ($y = 0$–0.7) samples were calculated in the case of 378 nm excitation and the results are shown in Fig. 12. The chromaticity coordinates of $Na_3Eu(PO_4)_2$ phosphor is also presented. The CIE chromaticity coordinates (X, Y) changes from point 1 (0.2987, 0.5695) to point 7 (0.6203, 0.3505) with the increase of Eu^{3+} concentration (y). The as formed $Na_3La_{0.95-x}(PO_4)_2$:xTb^{3+},$0.05Eu^{3+}$ ($x = 0$–0.95) phosphors show typical reddish-orange luminescence. However, their CIE coordinates are too close to be distinguished from each other in a chromaticity diagram with the changes of the Tb^{3+} ion concentration, so they are not presented.

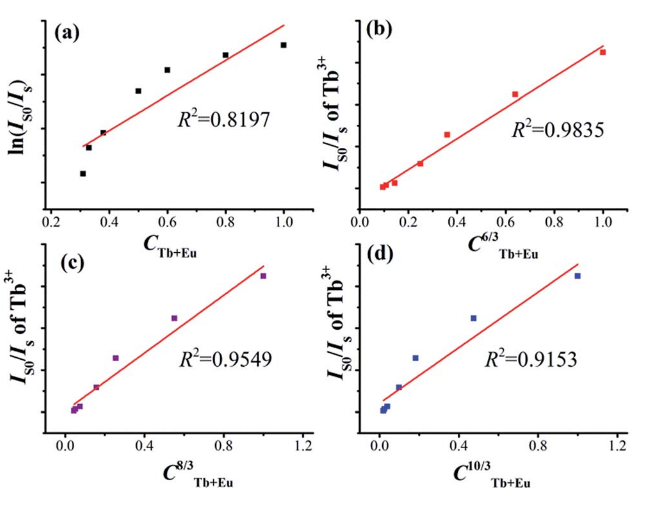

Fig. 10 Dependence of $\ln(I_{S0}/I_S)$ on C_{Tb+Eu} (a) and the dependence of I_{S0}/I_S on $C_{Tb+Eu}{}^{6/3}$ (b), $C_{Tb+Eu}{}^{8/3}$ (c) and $C_{Tb+Eu}{}^{10/3}$ (d).

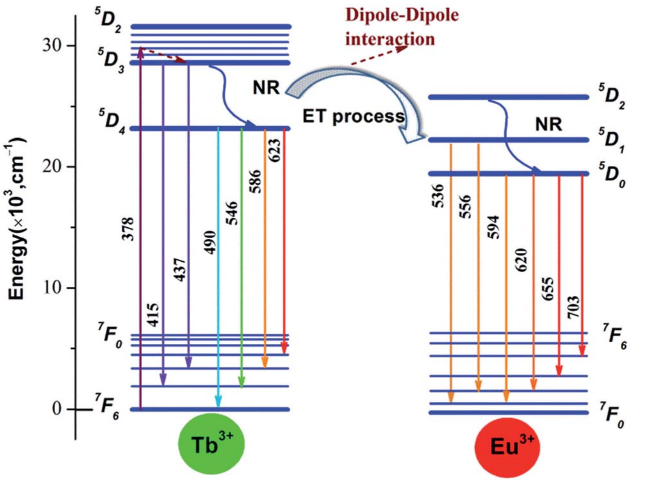

Fig. 11 Scheme of energy transfer from Tb^{3+} to Eu^{3+} in $Na_3La(PO_4)_2$ host.

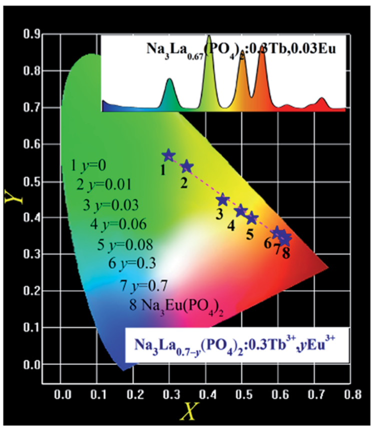

Fig. 12 CIE chromaticity diagram of the selected $Na_3La_{0.7-y}(PO_4)_2$:$0.3Tb^{3+}$,yEu^{3+} (y = 0–0.7) and $Na_3Eu(PO_4)_2$ phosphors under 378 nm UV irradiation excitation. The inset shows the PL spectrum of $Na_3La_{0.67}(PO_4)_2$:$0.3Tb^{3+}$,$0.03Eu^{3+}$ under 378 nm UV irradiation excitation.

The PL spectrum of $Na_3La_{0.67}(PO_4)_2$:$0.3Tb^{3+}$,$0.03Eu^{3+}$ phosphor shown as inset in Fig. 12 exhibits a green emission of the Tb^{3+} and the red emission of the Eu^{3+} ions. These emission lines of Tb^{3+} and Eu^{3+} cover the whole visible light region with tunable intensity, resulting in a color-tunable emission. Therefore, it can be expected to achieve color-tunable emission by regulating spectral composition induced by the energy transfer between Tb^{3+} and Eu^{3+} ions in the $Na_3La(PO_4)_2$ host under NUV irradiation excitation. According to Grassman's Laws of additive color mixture,[46,47] the emission color of $Na_3La(PO_4)_2$:Tb^{3+},Eu^{3+} can be matched by a linear combination of the emission color of $Na_3La(PO_4)_2$:Tb^{3+} and that of $Na_3La(PO_4)_2$:Eu^{3+}. It is obvious that the coordinate Y changes linearly with the coordinate X as shown in Fig. 12. Plotting y *vs.* x, a straight line is obtained. The values of intercept, slope, and linear regression coefficient are 0.7782, −0.7037, and 0.9902 respectively. The expression is shown as below:

$$Y = 0.7782 - 0.7037X \tag{10}$$

The above equation should mathematically demonstrate the range of chromaticity coordinates that we can obtain by adjusting the Tb^{3+} and Eu^{3+} concentrations. It is obvious that the chromaticity coordinates for the $Na_3La(PO_4)_2$:Tb^{3+},Eu^{3+} phosphor falls on a line connecting the two chromaticity coordinates of $Na_3La(PO_4)_2$:Tb^{3+} and $Na_3La(PO_4)_2$:Eu^{3+}, respectively. With increasing the Eu^{3+} concentration (y), the chromaticity coordinate for $Na_3La_{0.7-y}(PO_4)_2$:$0.3Tb^{3+}$,yEu^{3+} phosphors move from the chromaticity point 1 of $Na_3La_{0.7}(PO_4)_2$:$0.3Tb^{3+}$ toward point 8 of $Na_3Eu(PO_4)_2$ along this straight line. The prepared $Na_3La(PO_4)_2$:Tb^{3+},Eu^{3+} phosphor exhibits efficient tunable emission in the visible-light region upon excitation with NUV irradiation, and might find potential applications in multicolor displays and other optoelectronic devices.

Conclusions

In a conclusion, a series of Tb^{3+} and/or Eu^{3+} doped $Na_3La(PO_4)_2$ phosphors have been successfully synthesized and their luminescence properties have been investigated in detail. The glaserite-like orthorhombic structure provides the $Na_3La(PO_4)_2$ host the possibility of doping with Tb^{3+} or Eu^{3+} ions without substantial luminescence quenching. Tb^{3+} can efficiently sensitize Eu^{3+} emission under NUV excitation. The energy transfer mechanism ($Tb^{3+} \rightarrow Eu^{3+}$) was demonstrated to be dominated by a dipole–dipole interaction. The luminescence decay properties of Eu^{3+} in $Na_3La(PO_4)_2$:Tb^{3+},Eu^{3+} samples under $^7F_6$–$^5G_6$ excitation (378 nm) within Tb^{3+} ions were simulated with the energy transfer theory. The emission color of $Na_3La_{0.7-y}(PO_4)_2$:$0.3Tb^{3+}$,yEu^{3+} phosphors can be tunable from green through yellow and red region by adjusting the Eu^{3+} concentration. These results indicate that the as-synthesized phosphors may find potential applications as a color-tunable emitting material in solid state lighting.

Acknowledgements

This research was financially supported by "the Fundamental Research Funds for the Central Universities", South-Central University for Nationalities (CZY15002).

Notes and references

1 S. V. Eliseeva and J. C. G. Bünzli, *New J. Chem.*, 2011, **35**, 1165–1176.
2 T. Jüstel, H. Nikol and C. Ronda, *Angew. Chem., Int. Ed.*, 1998, **37**, 3084–3103.
3 C. Li, J. Yang, P. Yang, H. Lian and J. Lin, *Chem. Mater.*, 2008, **20**, 4317–4326.
4 T. Katsumata, K. Sasajima, T. Nabae, S. Komuro and T. Morikawa, *J. Am. Ceram. Soc.*, 1998, **81**, 413–416.
5 W.-R. Liu, C.-H. Huang, C.-W. Yeh, J.-C. Tsai, Y.-C. Chiu, Y.-T. Yeh and R.-S. Liu, *Inorg. Chem.*, 2012, **51**, 9636–9641.
6 R. P. Rao, *J. Lumin.*, 2005, **113**, 271–278.

7 T. Aitasalo, M. Guzik, W. Szuszkiewicz, J. Hölsä, B. Keller and J. Legendziewicz, *J. Alloys Compd.*, 2004, **380**, 405–412.
8 M. Kloss, B. Finke, L. Schwarz and D. Haberland, *J. Lumin.*, 1997, **72–74**, 684–686.
9 J. Matt Farmer, L. A. Boatner, B. C. Chakoumakos, C. J. Rawn and J. Richardson, *J. Alloys Compd.*, 2016, **655**, 253–265.
10 M. Guzik, T. Aitasalo, W. Szuszkiewicz, J. Hölsä, B. Keller and J. Legendziewicz, *J. Alloys Compd.*, 2004, **380**, 368–375.
11 J. Chékir-Mzali, K. Horchani-Naifer and M. Férid, *Superlattices Microstruct.*, 2015, **85**, 445–453.
12 H. Liang, Z. Tian, H. Lin, M. Xie, G. Zhang, P. Dorenbos and Q. Su, *Opt. Mater.*, 2011, **33**, 618–622.
13 A. Matraszek, P. Godlewska, L. Macalik, K. Hermanowicz, J. Hanuza and I. Szczygieł, *J. Alloys Compd.*, 2015, **619**, 275–283.
14 F. W. Kang, Y. Zhang and M. Y. Peng, *Inorg. Chem.*, 2015, **54**, 1462–1473.
15 F. Kang, Y. Zhang, L. Wondraczek, J. Zhu, X. Yang and M. Peng, *J. Mater. Chem. C*, 2014, **2**, 9850–9857.
16 F. Kang, H. Zhang, L. Wondraczek, X. Yang, Y. Zhang, D. Lei and M. Peng, *Chem. Mater.*, 2016, **28**, 2692–2703.
17 C.-H. Huang, P.-J. Wu, J.-F. Lee and T.-M. Chen, *J. Mater. Chem.*, 2011, **21**, 10489–10495.
18 M. Shang, D. Geng, D. Yang, X. Kang, Y. Zhang and J. Lin, *Inorg. Chem.*, 2013, **52**, 3102–3112.
19 K. Li, M. Shang, H. Lian and J. Lin, *J. Mater. Chem. C*, 2016, **4**, 5507–5530.
20 F. Kang, Y. Zhang and M. Peng, *Inorg. Chem.*, 2015, **54**, 1462–1473.
21 L. Li, Y. Liu, R. Li, Z. Leng and S. Gan, *RSC Adv.*, 2015, **5**, 7049–7057.
22 Q. Dan and T. Wanjun, *Ceram. Int.*, 2016, **42**, 1538–1544.
23 K. Li, S. Liang, M. Shang, H. Lian and J. Lin, *Inorg. Chem.*, 2016, **55**, 7593–7604.
24 J. Zhou and Z. Xia, *J. Mater. Chem. C*, 2014, **2**, 6978–6984.
25 A. C. Larson and R. B. Von Dreele, *Generalized Structure Analysis System (GSAS)*, Los Alamos National Laboratory, Los Alamos, NM, 1994, pp. 86–748.
26 R. D. Shannon, *Acta Crystallogr., Sect. A: Cryst. Phys., Diffr., Theor. Gen. Crystallogr.*, 1976, **32**, 751–767.
27 R. Salmon, C. Parent, M. Vlasse and G. Le Flem, *Mater. Res. Bull.*, 1978, **13**, 439–444.
28 W. D. Kingery, H. K. Bowen and D. R. Uhlmann, *Introduction to Ceramics*, Wiley, New York, 1976.
29 W. Liu, D. Wang, Y. Wang, J. Zhang and H. Tao, *J. Am. Ceram. Soc.*, 2013, **96**, 2257–2263.
30 G. Ju, Y. Hu, L. Chen, X. Wang, Z. Mu, H. Wu and F. Kang, *J. Alloys Compd.*, 2011, **509**, 5655–5659.
31 C. M. Liu, D. J. Hou, J. Yan, L. Zhou, X. J. Kuang, H. B. Liang, Y. Huang, B. B. Zhang and Y. Tao, *J. Phys. Chem. C*, 2014, **118**, 3220–3229.
32 X. Li, Y. Zhang, D. Geng, J. Lian, G. Zhang, Z. Hou and J. Lin, *J. Mater. Chem. C*, 2014, **2**, 9924–9933.
33 G. Blasse and B. C. Grabmaier, *Luminescent Materials*, Springer, Berlin, 1994.
34 P. Gupta, A. K. Bedyal, V. Kumar, Y. Khajuria, V. Kumar, E. Coetsee-Hugo, O. M. Ntwaeaborwa and H. C. Swart, *Opt. Mater.*, 2014, **36**, 996–1001.
35 B. R. Judd, *Phys. Rev.*, 1962, **127**, 750–761.
36 G. S. Ofelt, *J. Chem. Phys.*, 1962, **37**, 511–520.
37 G. R. Dillip, S. J. Dhoble, L. Manoj, C. M. Reddy and B. D. P. Raju, *J. Lumin.*, 2012, **132**, 3072–3076.
38 J. Legendziewicz, M. Guzik and J. Cybińska, *Opt. Mater.*, 2009, **31**, 567–574.
39 A. Pelczarska, A. Watras, P. Godlewska, E. Radominska, L. Macalik, I. Szczygieł, J. Hanuzaab and P. J. Deren, *New J. Chem.*, 2015, **39**, 8474–8483.
40 S. Chen, Y. Wang, J. Zhang, L. Zhao, Q. Wang and L. Han, *J. Lumin.*, 2014, **150**, 46–49.
41 T. Jiang, X. Yu, X. Xu, H. Yu, D. Zhou and J. Qiu, *Opt. Mater.*, 2014, **36**, 611–615.
42 Y. C. Li, Y. H. Chang, Y. S. Chang, Y. J. Lin and C. H. Laing, *J. Phys. Chem. C*, 2007, **111**, 10682–10688.
43 J. Zhong, H. Liang, Q. Su, J. Zhou, Y. Huang, Z. Gao, Y. Tao and J. Wang, *Appl. Phys. B*, 2010, **98**, 139–147.
44 F. Xie, J. Li, Z. Dong, D. Wen, J. Shi, J. Yan and M. Wu, *RSC Adv.*, 2015, **5**, 59830–59836.
45 R. Reisfeld, E. Greenberg, R. Velapoldi and B. Barnett, *J. Chem. Phys.*, 1972, **56**, 1698–1705.
46 H. Grassman, *Philos. Mag.*, 1854, **7**, 254–264.
47 W. Tang and Z. Zhang, *J. Mater. Chem. C*, 2015, **3**, 5339–5346.